ISSN 1674-1056
http://cpb.iphy.ac.cn
http://iopscience.iop.org/cpb
中国物理 B
Chinese Physics
中国物理
Chinese Physics B

Heat transfer of liquid metal alloy on copper plate deposited with film of different surface free energy

Huilong Yan(闫慧龙), Jinliang Yan(闫金良), Gang Zhao(赵刚)
Citation: Chin. Phys. B . 2019, 28(11): 114401 . **doi:** 10.1088/1674-1056/ab48dc
Journal homepage: http://cpb.iphy.ac.cn; http://iopscience.iop.org/cpb

What follows is a list of articles you may be interested in

Uniformity principle of temperature difference field in heat transfer optimization

Xue-Tao Cheng(程雪涛), Xin-Gang Liang(梁新刚)
Chin. Phys. B . 2019, 28(6): 064402 . **doi:** 10.1088/1674-1056/28/6/064402

Three-dimensional human thermoregulation model based on pulsatile blood flow and heating mechanism

Si-Na Dang(党思娜), Hong-Jun Xue(薛红军), Xiao-Yan Zhang(张晓燕), Jue Qu(瞿珏), Cheng-Wen Zhong(钟诚文), Si-Yu Chen(陈思宇)
Chin. Phys. B . 2018, 27(11): 114402 . **doi:** 10.1088/1674-1056/27/11/114402

Contribution of terahertz waves to near-field radiative heat transfer between graphene-based hyperbolic metamaterials

Qi-Mei Zhao(赵启梅), Tong-Biao Wang(王同标), De-Jian Zhang(张德建), Wen-Xing Liu(刘文兴), Tian-Bao Yu(于天宝), Qing-Hua Liao(廖清华), Nian-Hua Liu(刘念华)
Chin. Phys. B . 2018, 27(9): 094401 . **doi:** 10.1088/1674-1056/27/9/094401

Direct numerical simulation of viscoelastic-fluid-based nanofluid turbulent channel flow with heat transfer

Yang Juan-Cheng, Li Feng-Chen, Cai Wei-Hua, Zhang Hong-Na, Yu Bo
Chin. Phys. B . 2015, 24(8): 084401 . **doi:** 10.1088/1674-1056/24/8/084401

Flow and heat transfer of a nanofluid over a hyperbolically stretching sheet

A. Ahmad, S. Asghar, A. Alsaedi
Chin. Phys. B . 2014, 23(7): 074401 . **doi:** 10.1088/1674-1056/23/7/074401

Heat transfer of liquid metal alloy on copper plate deposited with film of different surface free energy*

Huilong Yan(闫慧龙)[1,†], Jinliang Yan(闫金良)[2,‡], and Gang Zhao(赵刚)[2]

[1] *Key Laboratory of Thermo-Fluid Science and Engineering (Ministry of Education), School of Energy and Power Engineering, Xi'an Jiaotong University, Xi'an* 710049, *China*

[2] *School of Physics and Optoelectronic Engineering, Ludong University, Yantai* 264025, *China*

(Received 15 April 2019; revised manuscript received 23 September 2019; published online 25 October 2019)

Liquid metal alloys (LMAs) are the potential candidates of thermal interface materials (TIMs) for electronics cooling. In the present work, buffer layers of Ag, Ti, Cu, Ni, Mo, and W were deposited on polished Cu plates by DC magnetron sputtering, the contact angles of de-ionized water and diiodomethane on the buffer layers were measured by an easy drop shape analyzer and the surface free energies (SFEs) of the buffer layers were calculated by the Owens–Wendt–Kaelble equation. Samples were prepared by sandwiching the filmed Cu plates and LMAs. The thermal properties of the samples were measured by laser flash analysis method. The SFE of the buffer layer has a strong influence on the interface heat transfer, whereas the measurement temperature has no obvious effect on the thermal properties of the samples. As the SFE of the buffer layer increases, the wettability, thermal diffusivity, and thermal conductivity are enhanced, and the thermal contact resistance is decreased.

Keywords: buffer layer, liquid metal alloy, thermal contact resistance, heat transfer, surface free energy

PACS: 44.10.+i, 68.08.–p, 65.40.gp, 68.08.Bc **DOI:** 10.1088/1674-1056/ab48dc

1. Introduction

In recent years, the continuous increase of extraordinary large amount of heat and especially the high heat flux generated in electronic chips made the thermal management a major serious concern throughout the world.[1,2] Therefore, it is critical to choose an efficient heat dissipation path to cool the electronic chip.[3] However, the cooling efficiency depends on the thermal contact quality of the interfaces. It is well known that when two solid surfaces are in contact, air pockets are created between the two solids at the interface due to asperities on each of the surfaces, low thermal conductivity air gaps result in thermal contact resistance (TCR). Thermal interface materials (TIMs) are needed to fill the air gaps to reduce the TCR between the interfaces.[4,5]

Commercial TIM is typically composed of a polymer matrix and conductive fillers. Metal oxide particles (MgO, Al_2O_3, etc.),[6] ceramics (SiC, BN, etc.),[7] and metals (Ag, Cu, Al, Ni, etc.)[8] have been widely adopted as fillers for conventional TIMs. Epoxy resin, rubber, and silicone are typical polymer matrices.[9] However, traditional TIMs exhibit low thermal conductivity even at high loading fractions. Carbon based TIMs have draw much attention in recent years. The axial thermal conductivity is 3000 W/mK for individual multiwalled carbon nanotubes (CNT).[10] However, the reported thermal conductivity of the CNT composites is rather unsatisfying.[11] Vertically aligned carbon nanotube (VACNT) films provide high conductivity in the axis and effectively transfer heat energy from a heat source to a heat sink, so VACNT films can be used as an attractive TIM in microelectronic packaging. Because of the poor bonding quality and high thermal resistance between VACNT tips and opposing surface, VACNTs are difficult to be used in high efficiency heat dissipation systems. As a two-dimensional material, the graphene has attracted a lot of attention due to its ultra high in-plane thermal conductivity in the range of 2000–5000 W/mK,[12] and is regarded as a promising filler to improve the thermal performance of the TIMs. However, the thermal conductivities of the graphene-based composites are still much lower than the expected value due to the interlayer thermal contact resistance.[13]

The liquid metal alloy (LMA) is a compound of gallium, indium, and tin, which is in liquid state below the operating temperature of the electronic component.[14,15] LMAs possess high thermal conductivity, and therefore are good candidates for the next generation TIMs.[16,17] However, the low wettability of LMAs on the heat sink may restrict its potential value in reducing cost and expanding use. In this study, the surface property of the Cu plate has been modified by coating films with different surface free energies (SFEs), and the heat transfer performance of LMAs on different SFE surfaces was investigated.

*Project supported by the National Natural Science Foundation of China (Grant No. 11874191) and the Natural Science Foundation of Shandong Province, China (Grant No. ZR2016FM38).

†Corresponding author. E-mail: 18742514109@163.com

‡Corresponding author. E-mail: yanjinliang8@sina.com

© 2019 Chinese Physical Society and IOP Publishing Ltd

2. Experimental details

2.1. Sample preparation

The polished oxygen-free Cu plates in 12.6 mm diameter were cleaned with acetone, ethanol, and hydrochloric acid solution (5% HCl & 95% water), and then rinsed in de-ionized water. Buffer layers of Ag, Ti, Ni, Cu, Mo, and W were deposited at room temperature on the Cu plates by DC magnetron sputtering. The sputtering chamber was first evacuated to a base pressure of 5×10^{-4} Pa, the sputtering was carried out under a pressure of 0.45 Pa in high purity argon flow of 20 sccm with a target-to-substrate distance of 65 mm. The sputtering power was fixed at 32 W, a continuous and homogeneous buffer layer with 60 nm thickness was formed on the Cu plate by controlling the sputtering time. LMA of $Ga_{62.5}In_{21.5}Sn_{16}$, which was purchased from Indium Corporation with melting point of 10.7 °C, was used as TIM. It was scrubbed on the surface of the filmed plate using a small brush, then two plates were stacked up and pressed to form a sandwiched structure sample, as shown in Fig. 1.



Fig. 1. Schematic of the sandwiched structure.

2.2. Characterization

The nominal film thickness as well as the deposition rate were monitored with a quartz crystal thickness monitor. The film thicknesses were checked using a surface profilometer, and good agreement was obtained. The drop shape analyzer (KRUSS GmbH) was used for measuring the contact angles of de-ionized water and diiodomethane on the filmed Cu plates, in which the contact angles of droplets with volume of 4 μl were measured and calculated using the sessile drop method and Young–Laplace fitting after the steady state was reached.

The laser flash analyzer (LFA 457, NETZSCH) was used to investigate the thermal properties of the samples. The detailed specification of LFA 457 can be found elsewhere.[18] The thermal conductivity (k) of the sample was calculated from the specific heat capability C_p, thermal diffusivity α, and sample density ρ using the relation $k=\alpha\rho C_p$. The thermal diffusivity of the sample was obtained by fitting the temperature risen curve. The sample density was calculated by measuring its volume and weight. The specific heat capacity could be obtained by a comparative method wherein two samples were measured at the same time: a sample prepared in this paper, and a reference sample with previously determined properties. The TCR could be obtained from the thermal conductivity and physical parameters of the samples.

3. Results and discussion

3.1. Contact angle and wettability

De-ionized water and diiodomethane are selected as a probe for the SFE calculations because they have a well-known value of surface tension, polar component and dispersion component. Values presented in Table 1 are used in the calculation of SFE by the method of Owens–Wendt–Rabel–Kaelbl.[19] The contact angles of de-ionized water and diiodomethane on the filmed copper plates are shown in Figs. 2 and 3. After sputtering films on the Cu plates, the contact angles of de-ionized water and diiodomethane change with the coating materials. This experiment shows how the wettability of liquid on solid can be controlled by coating.

Table 1. Surface tension parameters of deionized water and diiodomethane.

Type	surface tension γ_l/mN·m^{-1}	Polar component γ_l^p/mN·m^{-1}	Dispersion component γ_l^d/mN·m^{-1}
De-ionized water	72.8	51.0	21.8
Diiodomethane	50.8	1.3	49.5

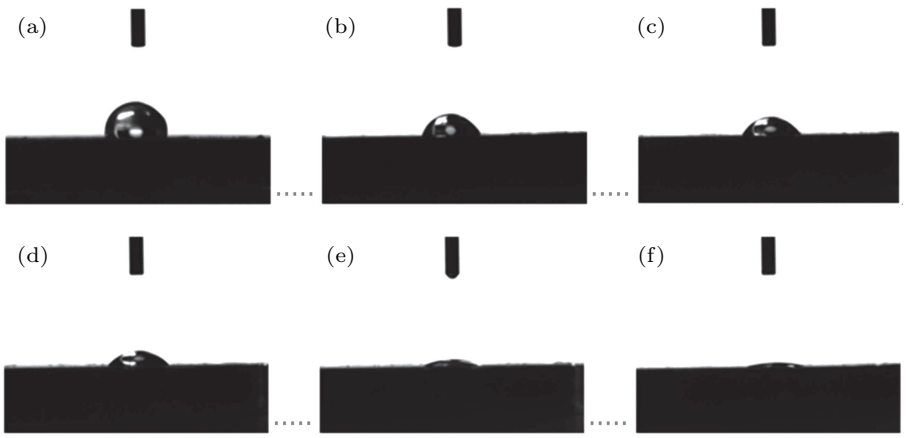


Fig. 2. Contact angle of de-ionized water on filmed Cu plate: (a) Ag coating (101.8°), (b) Ti coating (78.9°), (c) Cu coating (65.9°), (d) Ni coating (51.9°), (e) Mo coating (17.8°), (f) W coating (6.8°).

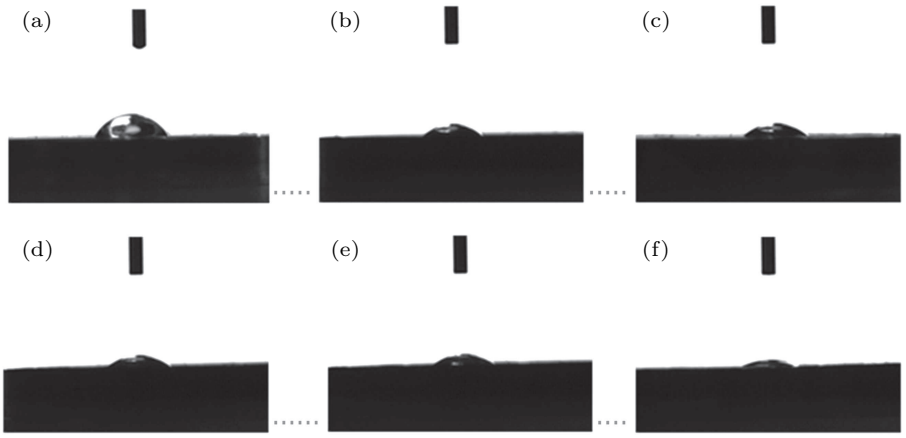


Fig. 3. . Contact angle of diiodomethane on filmed Cu plate: (a) Ag coating (64.6°), (b) Ti coating (43.4°), (c) Cu coating (41.8°), (d) Ni coating (36.8°), (e) Mo coating (29.3°), (f) W coating (19.1°).

For calculating SFE, the geometric mean approach was used to combine the dispersion and polar components by the method of Owens, Wendt, Rabel, and Kaelble. It is assumed that the total SFE of solid and liquid is merely a sum of both polar and dispersion components in this model.[20] Based upon the above data, the SFE of the buffer layer deposited on Cu plate was calculated using the Owens–Wendt–Kaelble equation, which is followed by ASME D7490-13, as follows:

$$\frac{\gamma_{\rm l}(1+\cos\theta)}{2} = \left[\left(\gamma_{\rm l}^{\rm d}\gamma_{\rm s}^{\rm d}\right)^{1/2} + \left(\gamma_{\rm l}^{\rm p}\gamma_{\rm s}^{\rm p}\right)^{1/2}\right], \qquad (1)$$

where θ (°) is the contact angle of reagent on the filmed Cu plate, and $\gamma_{\rm l}$ is the surface tension of the used reagent. $\gamma_{\rm l}^{\rm d}$ and $\gamma_{\rm l}^{\rm p}$ are the dispersion component and polar component of liquid surface tension, $\gamma_{\rm s}^{\rm d}$ and $\gamma_{\rm s}^{\rm p}$ are the dispersion component and polar component of SFE for the filmed Cu plate. The total SFE and its components for the filmed Cu plates are shown in Table 2. The highest value of SFE is obtained for the W film and the lowest for the Ag film. In addition, a relationship is build in the values of contact angles and SFEs, the contact angle decreases with increasing SFE. According to our research, we are able to forecast that the buffer layers with higher SFEs will build the stronger wettability than the buffer layers with lower SFEs. In reality, the actual SFE is affected by many factors. However, the SFE calculation clearly points out the correlation between the SFE and coating composition. Wettability can be modified by coating different materials on the copper plates.

Table 2. Surface free energy (in mN·m^{-1}) of buffer layer deposited on Cu plate.

Buffer layer	Surface free energy	Dispersion part	Polar part
Ag	25.93	25.35	0.58
Ti	40.16	35.36	4.80
Cu	44.21	32.16	12.05
Ni	53.31	33.38	19.93
Mo	71.41	33.13	38.28
W	74.93	36.15	38.78

3.2. Thermal properties

Figure 4 presents the thermal diffusivities of the samples at different measurement temperatures. It is obvious from Fig. 4 that the thermal diffusivities of the samples have no significant change with the measurement temperature, which should be attributed to no phase change of the LMA in the major operation temperature range of electronics. A distinct difference is observed in the data of thermal diffusivities among the sandwiched structure samples, the thermal diffusivity is different for the sample with different buffer layer. For the Cu coated sample, the average thermal diffusivity is 97.673 mm^2/s, the average thermal diffusivities are 90.314 mm^2/s and 93.777 mm^2/s respectively for the Ag coated sample and the Ti coated sample, which are 7.5% and 4.0% lower than that of the Cu coated sample. For the samples coated with Ni, Mo, and W, the average thermal diffusivities are 99.771 mm^2/s, 102.922 mm^2/s, and 105.482 mm^2/s, which are 2.15%, 5.37%, and 8.0% higher than that of the Cu coated sample, respectively. Combined with Table 2 and Fig. 4, it can be seen that the thermal diffusivity of the sample is strongly dependent on the SFE of the buffer layer, with a higher SFE consistently resulting in higher thermal diffusivity. In practice, it is noted that the surface coated with higher SFE film is more easily wetted with LMA, while the surface coated with lower SFE film is hard scrubbed with the alloy using a cotton swab to induce wetting. On the microscopic level, in case of a surface with good wettability, LMA could easily flow and fill in the uneven area on the filmed Cu plate, the true contact area between the LMA and buffer layer is increased, which means the thermal diffusivity is also increased with improving the wettability of LMA on buffer layer. So, the SFE of the buffer layer has a great effect on the thermal diffusivity of the sample.

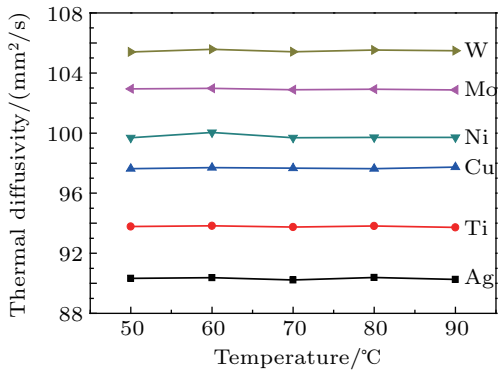


Fig. 4. Thermal diffusivity of the sample at different temperatures.

Figure 5 displays the thermal conductivities of the samples measured at different temperatures. The average thermal conductivity of the Cu coated sample is 350.443 W/mK, the thermal conductivities of the Ag coated sample and the Ti coated sample are lower, which are 324.152 W/mK and 335.822 W/mK, respectively. The average thermal conductivities are 357.846 W/mK, 369.488 W/mK, and 378.305 W/mK for the samples coated with Ni, Mo, and W. There is large difference in the data of thermal diffusivities caused by the insertion of different SFE buffer layers. The buffer layer in the interface region can modify the thermal transfer. As shown in Fig. 5, the sample measurement temperature has little effect on the thermal conductivity, whereas the thermal conductivity increases monotonically with the SFE of the buffer layer. Even a small change in SFE would result in observable change in thermal conductivity. The wettability of LMA on a surface affects the real contact area. The surface with high SFE can form more continuous thermal conductive pathways in the interface region and thus be more effective in enhancing the heat transfer.

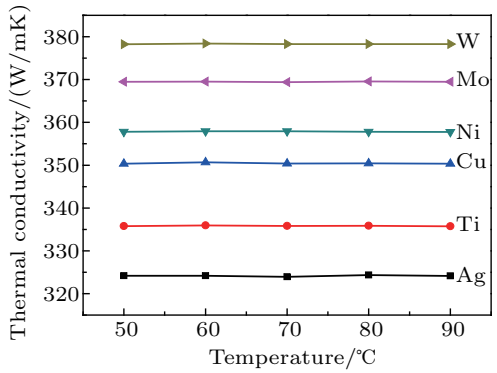


Fig. 5. Thermal conductivity of the sample at different temperatures.

Figure 6 presents TCRs of samples at different measurement temperatures. Clearly, the TCR of the sample varies little with measurement temperature. The TCR of the Cu coated sample is as low as 1.119 mm^2 K/W. Compared with the Cu coated sample, the TCRs of the samples coated with Ni, Mo, and W are 0.917 mm^2·K/W, 0.617 mm^2·K/W, and 0.4 mm^2·K/W, which are decreased respectively by about 18.05%, 44.86%, and 64.25%; on the contrary, the TCRs of the Ti coated sample and the Ag coated sample are increased by about 36.28% and 70.15%, which are 1.525 mm^2·K/W and 1.904 mm^2·K/W. The variation in TCR comes from the different buffer layers. The TCR of the sandwiched sample consists of five parts, namely, the bulk thermal resistance of the LMA layer, the two LMA/buffer layer interfacial thermal resistances, and the two thermal resistances of the buffer layers. The metal buffer layer is too thin and its thermal resistance can be ignored. Since the thermal conductivity of LMA is relatively high and the amount of LMA is negligible, the bulk thermal resistance of the LMA layer is also negligible. Hence the TCR results from the total interfacial thermal resistances. The interfacial thermal resistances depend on the quality of the contact between the LMA and buffer layer. The TCR decreases monotonically by increasing SFE of the buffer layer, as shown in Fig. 6 and Table 2. This means that the TCR can be modified using different SFE buffer layers on copper plates.

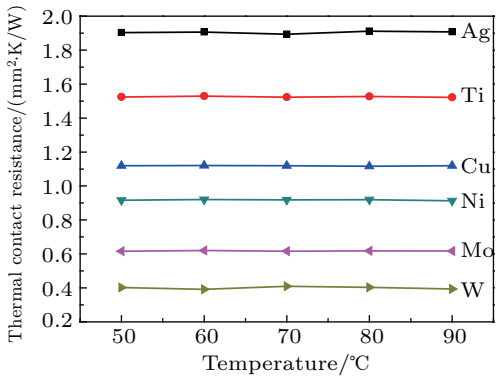


Fig. 6. Thermal contact resistance of the sample at different temperature.

As we know, electrons dominate the thermal conduction in LMA/buffer layer, so energy transfer must occur between electrons in LMA and electrons in buffer layer. During the wetting procedure, high SFE buffer layer could promote LMA wettability,[21] which can improve the necessary electron–electron collision in the interfacial regions and heat transport pathways. This directly reduces the two interfacial thermal resistances, facilitating the achievement of low TCR. As expected, a buffer layer influences the wettability of LMA on the plate surface and interfacial thermal resistance, high SFE buffer layer can enhance the thermal transfer and facilitate the achievement of low interfacial thermal resistance.

4. Conclusion

Buffer layers of Ag, Ti, Cu, Ni, Mo, and W were deposited on polished Cu plates to investigate interfacial heat transfer. The buffer layer influences the LMA wettability, thermal diffusivity, thermal conductivity, and TCR of the samples. The thermal diffusivity, thermal conductivity, and TCR

of the samples have no significant change with the measurement temperature. The wettability, thermal diffusivity, and thermal conductivity are enhanced with increasing the SFE of the buffer layer, the TCR is decreased monotonically by increasing the SFE of the buffer layer. High SFE buffer layer could promote LMA wettability, which can improve the necessary electron–electron collision in the interfacial regions and heat transport pathways. High SFE buffer layer can enhance the thermal transfer and facilitate the achievement of low interfacial thermal resistance.

References

[1] Zhang Z W and Chen J 2018 *Chin. Phys. B* **27** 035101

[2] Sarafraz M M, Arya A, Hormozi F and Nikkhah V 2017 *Appl. Therm. Eng.* **112** 1373

[3] Yang X H and Liu J 2018 *Adv. Heat Transfer.* **50** 187

[4] McNamara A J, Joshi Y and Zhang Z M 2012 *Int. J. Therm. Sci.* **62** 2

[5] Mei S F, Gao Y X, Deng Z S and Liu J 2014 *ASME J. Electron. Packag.* **136** 011009

[6] Sim L C, Ramanan S R, Ismail H, Seetharamu K N and Goh T J 2005 *Thermochim. Acta* **430** 155

[7] Yuan C, Xie B, Huang M Y, Wu R K and Luo X B 2016 *Int. J. Heat Mass Tran.* **94** 20

[8] Wang S, Cheng Y, Wang R, Sun J and Gao L 2014 *ACS Appl. Mater. Interfaces* **6** 6481

[9] Zhang P, Li Q and Xuan Y M 2014 *Compos. Part. A-Appl. S.* **57** 1

[10] Yu C H, Shi L, Yao Z, Li D Y and Majumdar A 2005 *Nano Lett.* **5** 1842

[11] Nylander A N, Fu Y F, Huang M L and Liu J 2019 *IEEE Trans. Compon. Packag. Manuf. Technol.* **9** 427

[12] Wang C Y, Lu S, Yu X D and Li H P 2019 *Chin. Phys. B* **28** 016501

[13] Renteria J, Legedza S, Salgado R, Balandin M P, Ramirez S, Saadah M, Kargar F and Balandina A A 2015 *Mater. Des.* **88** 214

[14] Yang E, Guo H Y, Guo J D, Shang J K and Wang M G 2014 *Acta Metall. Sin. (Eng. Lett.)* **27** 290

[15] Ma K Q and Liu J 2007 *Front. Energy Power Eng. Chin.* **1** 384

[16] Gao Y X and Liu J 2012 *Appl. Phys. A* **107** 701

[17] Gao Y X, Wang X P, Liu J and Fang Q F 2017 *ASME J. Electron. Packag.* **139** 011002

[18] Min S, Blumm J and Lindemann A 2007 *Thermochim. Acta* **455** 46

[19] Fan C W and Lee S C 2007 *Mater. Trans.* **48** 2449

[20] Fernando P S G, Daniel Y, Charles M, Ryo J, Nick T, Darceny Z B and Paulo G C 2013 *Int. J. Biomater.* **2013** 354125

[21] Tao Z C, Guo Q G, Gao X Q and Liu L 2011 *Mater. Chem. Phys.* **128** 228